IEEE Photonics Journal
An IEEE Photonics Society Publication

4-by-4 Integrated Waveguide Coupler Based on Bi-Directional Propagation in Two Single-Mode Waveguides

Volume 13, Number 1, February 2021

Mathias J. Weisen
James C. Gates
Corin B. E. Gawith, *Member, IEEE*
Peter G. R. Smith
Peter Horak

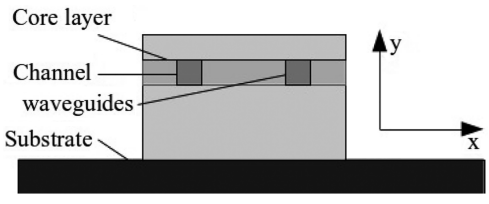

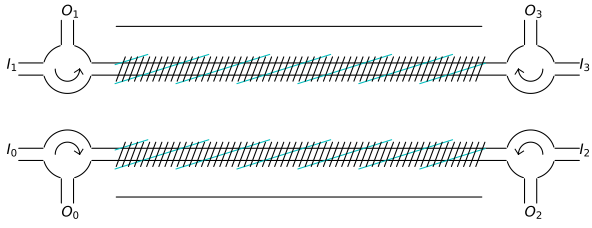

DOI: 10.1109/JPHOT.2020.3040073

4-by-4 Integrated Waveguide Coupler Based on Bi-Directional Propagation in Two Single-Mode Waveguides

Mathias J. Weisen, James C. Gates, Corin B. E. Gawith, *Member, IEEE*, Peter G. R. Smith, and Peter Horak

Optoelectronics Research Centre, University of Southampton, Southampton, SO17 1BJ, UK

DOI:10.1109/JPHOT.2020.3040073

Manuscript received July 23, 2020; revised November 16, 2020; accepted November 19, 2020. Date of publication November 24, 2020; date of current version February 8, 2021. This work was supported by the Engineering and Physical Sciences Research Council (EPSRC) Quantum Technology Programme (EP/M013243/1, EP/M013294/1, EP/T001062/1) and an EPSRC PhD studentship. Corresponding author: Mathias J. Weisen (e-mail: m.j.weisen@soton.ac.uk).

Abstract: We propose and investigate theoretically the use of bi-directional propagation of light in silica integrated coupled waveguide structures for linear optical processing of fiber-coupled photons. We show that the class of linear operations that can be implemented in such a system is given by symmetric and unitary matrices. We present how an arbitrary 4×4 coupler of this form can be realized by a linear sequence of more fundamental 2×2 couplers and single-waveguide phase shifters and discuss in detail the implementation in a silica integrated platform utilizing direct UV-written waveguides and long- and short-period grating couplers with tilted gratings for optimized coupling efficiency.

Index Terms: Bragg gratings, optical waveguides, quantum processing.

1. Introduction

The use of photonic technology for quantum information processing has been the topic of extensive research [1]. Of particular interest are integrated photonic platforms for the manipulation of quantum states, typically using an architecture based on directional couplers between multiple waveguides [2]–[4]. For example, a C-NOT gate [5]–[7], fast Fourier transforms [8], and quantum transport simulations [9] have been demonstrated with this technology.

More generally, this platform has been used to implement universal linear optics [4], i.e., to implement any linear, classical transformation of light modes represented mathematically by a $N \times N$ unitary matrix, where the condition for a unitary matrix represents a lossless device. This is achieved by decomposing the unitary matrix into a product of simple transformations that can be implemented by directional couplers [10]–[12].

These implementations have so far only been made using a single propagation direction with directional couplers based on evanescent field coupling between waveguides. However, other directional couplers exist that utilize Bragg gratings, for example to assist waveguide-to-waveguide coupling in a frequency selective way [13] or for wavelength division multiplexers [14], [15]. Directional couplers have also been constructed as long-period waveguide grating couplers [16]–[18] that use a forward propagating cladding mode as an intermediary “bus” mode. This has been

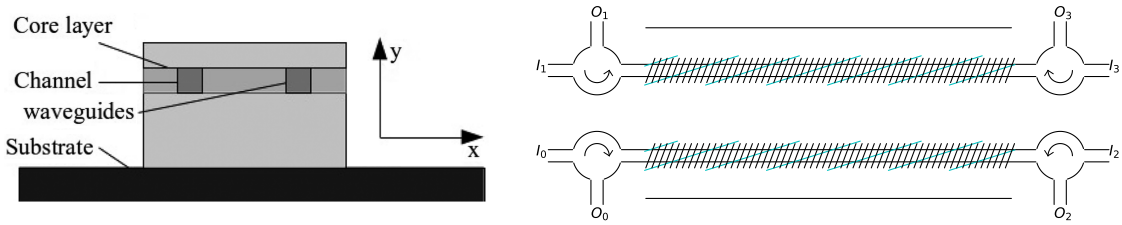

Fig. 1. Left: Cross section of the device in the transverse direction showing the higher refractive index photosensitive core layer with two single-mode waveguides and top and bottom cladding layers. Right: Top view of the core layer showing the two waveguides with incorporated tilted long- and short-period Bragg gratings. Also shown are the optical circulators to separate input and output channels.

proposed as a possible basis for constructing a Walsh-Hadamard transform [19]. Recently we also demonstrated an extension of this scheme in a silica platform exploiting UV-written tilted Bragg gratings and higher order cladding modes in the backward direction for enhanced wavelength selectivity [20].

Here we target in particular linear operations on a small number of fiber-coupled narrow bandwidth light pulses, e.g, for applications in optically connected quantum networks [21]. Direct UV-written waveguides in a planar silica platform provide an ideal implementation of such devices since they allow for fiber coupling with small insertion loss of 0.1 dB [22] and low propagation losses of 0.2 dB/cm [23], [24]. With direct UV-writing technology it is also possible to simultaneously inscribe waveguides and Bragg gratings [25].

In order to minimize the number of waveguides required, while still maintaining single-mode operation, we here propose the use of both forward and backward propagating modes in UV-written silica waveguides, thereby doubling the number of input and output channels compared to uni-directional systems. However, since every waveguide coupler affects light propagating in both directions, not every arbitrary unitary input-output transfer matrix can be achieved in this system. Instead, we show in the case of 4 input and 4 output modes (i.e., two forward and two backward propagating modes) that every *symmetric* unitary 4×4 matrix can be realized.

Specifically, we consider two UV-written single-mode waveguides contained in a single silica ridge structure that confines light in the transverse direction in multiple cladding modes. Both propagation directions of the two waveguides are exploited, leading to a device with four input and output ports. Tilted gratings are used to couple between all input and output ports via a single high-order cladding mode. Light is coupled to and from each of the ports to optical fibers and the inputs and outputs are separated via optical circulators. We identify a set of fundamental mode couplers that can be concatenated to build up any symmetric and unitary transfer matrix, simulate their implementation, and discuss the realization of several optical processors (Walsh-Hadamard, quantum Fourier transform, CNOT gates).

2. Device Geometry and Theoretical Description

We show a schematic of the proposed device geometry in Fig. 1. It consists of a single silica ridge structure which can be fabricated e.g. by micromachining two parallel trenches in a planar substrate [26]. The ridge structure contains a photosensitive germanosilicate planar core layer with raised refractive index surrounded by top and bottom claddings. Light in this layer is confined to a single mode vertically, but is able to support a number of discrete modes in the transverse direction with well-separated effective mode index. Through direct UV writing [25] two parallel single-mode waveguides are written into the core layer. In the following we refer to the guided modes of the waveguides as “core modes” and to those guided by the core layer as “cladding modes”. Note that these cladding modes are bound in the vertical direction by the higher refractive index of the core layer compared to the surrounding silica and in the transverse direction by the glass-air interfaces of the ridge.

Light from an optical fiber can be coupled at both ends into the two waveguides using waveguide-to-fiber interconnects with high modal coupling [22]. Likewise, the device output occurs at both ends of the waveguides back into the fiber and these outputs are separated from the inputs via four optical circulators as indicated in Fig. 1. Bragg gratings are written by the same direct UV writing technique into the two waveguides and are used to couple light between the forward and backward propagating modes of the two waveguides by using a cladding mode as an intermediary. By carefully choosing the grating parameters we can achieve arbitrary waveguide-to-waveguide coupling ratios while simultaneously ensuring that none of the light escapes via the cladding modes at the input and output ends of the device, see Sec. III.

Two types of Bragg gratings are used in the device: short-period gratings for coupling of waveguide modes to counter-propagating cladding modes and long-period gratings to couple to co-propagating cladding modes. The gratings are designed for phase matching and, via tilted grating planes, for optimized coupling efficiency to a single cladding mode in order to avoid interference from light coupled via other cladding modes which would reduce the performance of the device. Details of this coupling scheme can be found in Ref. [20]. The combination of short- and long-period gratings allows us to couple light between all four input and output ports. We aim to achieve as wide a range of 4×4 coupling matrices on a single chip as possible, either with a single device or by concatenating individual, more fundamental couplers on a single chip. In either case, the waveguides are coupled to optical fibers at the edge of the chip.

The use of a single-mode core layer allows us to simplify the problem from three to two dimensions using the effective index method [27].

We model this device using coupled mode theory. We first calculate all optical eigenmodes of the structure using a finite differences method and then the coupling coefficients of each grating using the overlap integrals between the core and the cladding modes. Light propagation along all modes is then calculated by solving the coupled mode equations as an eigenvalue/eigenvector problem.

In the following we will assume that light is coupled from the waveguide modes to a *single* forward and backward propagating cladding mode. Such selective coupling is achieved by phase matching with narrow bandwidth gratings of mm to cm length [23], [25], [28], as we will discuss in Sec. VII. With direct UV writing, the gratings are created using the interference pattern of two laser beams and so in principle can be made perfectly sinusoidal, which minimizes higher diffraction orders that could cause unwanted coupling to other cladding modes. Coupled mode theory including *all* cladding modes in this geometry has previously also confirmed that the approximation of a single coupled cladding mode is well justified for the chosen parameters [20] and comparisons of calculated coupling coefficients with full finite element simulations of tilted Bragg gratings have shown excellent agreement [28].

We denote the amplitudes of the light fields propagating in the device by R_n where $n = 0, 1$ refers to the forward propagating modes of waveguide 0 and 1, $n = 2, 3$ refer to the corresponding backward propagating modes and $n = 4, 5$ refer to the forward and backward propagating cladding mode that is used as a bus. The coupled mode equations can then be written as

$$\frac{d}{dz}\mathbf{R}(z) = M \cdot \mathbf{R}(z) \tag{1}$$

where $\mathbf{R}$ is a column vector of the amplitudes R_n and

$$M = \begin{bmatrix} \cdot & \cdot & \cdot & \cdot & -\frac{1}{2}g_2^* & -\frac{1}{2}g_0 \\ \cdot & \cdot & \cdot & \cdot & -\frac{1}{2}g_3^* & -\frac{1}{2}g_1 \\ \cdot & \cdot & i\Delta K_t & \cdot & -\frac{1}{2}g_0^* & -\frac{1}{2}g_2 \\ \cdot & \cdot & \cdot & i\Delta K_t & -\frac{1}{2}g_1^* & -\frac{1}{2}g_3 \\ \frac{1}{2}g_2 & \frac{1}{2}g_3 & -\frac{1}{2}g_0 & -\frac{1}{2}g_1 & i\Delta K_h & \cdot \\ -\frac{1}{2}g_0^* & -\frac{1}{2}g_1^* & \frac{1}{2}g_2^* & \frac{1}{2}g_3^* & \cdot & -i\Delta K \end{bmatrix}. \tag{2}$$

Here g_0 and g_1 are the coupling coefficients of the short-period gratings in waveguides 0 and 1 respectively, g_2 and g_3 are the coupling coefficients of the long-period gratings, "*" denotes the

complex conjugate, and "·" denotes empty matrix elements. $\Delta K_t = \Delta K_h - \Delta K$ and ΔK and ΔK_h are the phase mismatch of the short- and long-period waveguide gratings defined by $\Delta K = -\beta_{\text{core}} - \beta_{\text{clad}} + K_g$ and $\Delta K_h = \beta_{\text{core}} - \beta_{\text{clad}} - K_h$ where β_{core} and β_{clad} are the propagation constants of the core modes and the cladding mode, respectively, and K_g and K_h are the grating wavenumbers of the short- and long-period gratings, respectively. While for arbitrary values of the parameters g_n, K_g, and K_h Eq. (1) can only be solved numerically, we will discuss some special analytically solvable cases in the next section. We also note that for simplicity we here assume lossless light propagation in our device. However, realistic losses of e.g. 0.2 dB/cm in silica waveguides [23], [24] will not qualitatively change the results and conclusions derived below.

Note that the waveguides are generally birefringent and we only consider vertically polarized (y-polarized) modes. The device can also be designed for the other polarization by appropriate choices of grating parameters.

In principle, this device could also be realized in an all-fiber implementation using a fiber with multiple cores. However, it would be difficult to write gratings of different grating period and tilt angle in different cores in a fiber geometry.

3. Analytical Solutions

In this and the following sections we will restrict our analysis to the case with exact phase matching for both the short- and long-period gratings, i.e., $\Delta K = \Delta K_h = 0$. By analytically computing the eigenvalues and eigenvectors of M, Eq. (2), we find that the general solution of Eq. (1) is:

$$\begin{bmatrix} R_0(z) \\ R_1(z) \\ R_2(z) \\ R_3(z) \\ R_4(z) \\ R_5(z) \end{bmatrix} = p_0 \begin{bmatrix} |g_3|^2 - |g_1|^2 \\ g_1\, g_0^* - g_2\, g_3^* \\ \cdot \\ g_3\, g_0^* - g_2\, g_1^* \\ \cdot \\ \cdot \end{bmatrix} + p_1 \begin{bmatrix} g_3\, g_2^* - g_0\, g_1^* \\ |g_0|^2 - |g_2|^2 \\ g_3\, g_0^* - g_2\, g_1^* \\ \cdot \\ \cdot \\ \cdot \end{bmatrix} + q_0 \begin{bmatrix} g_0 \\ g_1 \\ g_2 \\ g_3 \\ \cdot \\ 2\gamma \end{bmatrix} e^{-\gamma z} + q_1 \begin{bmatrix} g_2^* \\ g_3^* \\ g_0^* \\ g_1^* \\ 2\gamma \\ \cdot \end{bmatrix} e^{-\gamma z}$$
$$+ q_2 \begin{bmatrix} g_0 \\ g_1 \\ g_2 \\ g_3 \\ \cdot \\ -2\gamma \end{bmatrix} e^{\gamma z} + q_3 \begin{bmatrix} g_2^* \\ g_3^* \\ g_0^* \\ g_1^* \\ -2\gamma \\ \cdot \end{bmatrix} e^{\gamma z} \tag{3}$$

where $\gamma = \frac{1}{2}\sqrt{|g_0|^2 + |g_1|^2 - |g_2|^2 - |g_3|^2}$ and p_0, p_1, q_0, q_1, q_2 and q_3 are arbitrary coefficients. We can see that the device has two regimes of behavior, one for $|g_0|^2 + |g_1|^2 > |g_2|^2 + |g_3|^2$ in which the contribution from the short-period gratings dominates, a photonic bandgap opens up and the light decays exponentially along its propagation direction. The other regime is for $|g_0|^2 + |g_1|^2 < |g_2|^2 + |g_3|^2$ where the long-period gratings dominate and no photonic bandgap occurs, leading to the fields oscillating with a single spatial frequency defined by

$$\Omega = -i\gamma = \frac{1}{2}\sqrt{|g_2|^2 + |g_3|^2 - |g_0|^2 - |g_1|^2}. \tag{4}$$

At the interface between these two regimes, for $\gamma = 0$, all the eigenvalues are zero, and the matrix M becomes defective. Such a device operates at the very edge of the bandgap and becomes very sensitive to phase mismatch.

Next, we set the boundary conditions such that no light enters the cladding modes at the device ends and also no light escapes via the cladding modes at $z = 0$ and $z = L$ where L is the length of

the device:

$$R_4(0) = R_4(L) = R_5(0) = R_5(L) = 0. \tag{5}$$

This is only possible in the oscillatory regime and from Eq. (3) we obtain the conditions $q_- \equiv q_0 = q_2$, $q_+ \equiv q_1 = q_3$, and $\sin(\Omega L) = 1$, i.e.,

$$\Omega L = m\pi, \tag{6}$$

where m is an integer number. The z-dependence of the waveguide mode amplitudes is then given by

$$\begin{bmatrix} R_0(z) \\ R_1(z) \\ R_2(z) \\ R_3(z) \end{bmatrix} = p_0 \begin{bmatrix} |g_3|^2 - |g_1|^2 \\ g_1\, g_0^* - g_2\, g_3^* \\ \cdot \\ g_3\, g_0^* - g_2\, g_1^* \end{bmatrix} + p_1 \begin{bmatrix} g_3\, g_2^* - g_0\, g_1^* \\ |g_0|^2 - |g_2|^2 \\ g_3\, g_0^* - g_2\, g_1^* \\ \cdot \end{bmatrix} + 2 \left(q_- \begin{bmatrix} g_0 \\ g_1 \\ g_2 \\ g_3 \end{bmatrix} + q_+ \begin{bmatrix} g_2^* \\ g_3^* \\ g_0^* \\ g_1^* \end{bmatrix} \right) \cos(\Omega z) \tag{7}$$

and that of the cladding modes by

$$\begin{bmatrix} R_4(z) \\ R_5(z) \end{bmatrix} = -2i \begin{bmatrix} q_- \\ q_+ \end{bmatrix} \Omega \sin(\Omega z). \tag{8}$$

In order to have a non-trivial solution, the fields should be different at both ends of the device and thus m should be an odd number such that $\cos(\Omega L) = -1$.

The device inputs I_m and outputs O_m as shown in Fig. 1 are then given by

$$\begin{aligned} I_0 = R_0(0),\ I_1 = R_1(0),\ I_2 = R_2(L),\ I_3 = R_3(L), \\ O_0 = R_2(0),\ O_1 = R_3(0),\ O_2 = R_0(L),\ O_3 = R_1(L). \end{aligned} \tag{9}$$

In later parts of the paper we will use two different ways of defining transfer matrices in our device. The first method relates the light at the output ports to the input ports by the following scattering matrix denoted as S,

$$\begin{bmatrix} O_0 \\ O_1 \\ O_2 \\ O_3 \end{bmatrix} = S \begin{bmatrix} I_0 \\ I_1 \\ I_2 \\ I_3 \end{bmatrix}. \tag{10}$$

With reference to Fig. 1, it is clear that this matrix must be symmetric as a result of the Lorentz reciprocity theorem [29] and unitary if we assume it to be lossless. The second method relates the light at the right hand side to the light at the left hand side of the device by a transfer matrix denoted as Σ such that

$$\begin{bmatrix} O_2 \\ O_3 \\ I_2 \\ I_3 \end{bmatrix} = \Sigma \begin{bmatrix} I_0 \\ I_1 \\ O_0 \\ O_1 \end{bmatrix}. \tag{11}$$

Throughout this paper we will call this second form the "unidirectional matrix". To relate the two types of transformation matrices we write the matrix S in terms of 2×2 submatrices,

$$S = \begin{bmatrix} S_{00} & S_{01} \\ S_{10} & S_{11} \end{bmatrix}. \tag{12}$$

The corresponding unidirectional matrix Σ is then given by

$$\Sigma = \begin{bmatrix} S_{10} - S_{11}S_{01}^{-1}S_{00} & S_{11}S_{01}^{-1} \\ -S_{01}^{-1}S_{00} & S_{01}^{-1} \end{bmatrix}. \tag{13}$$

For any given input light amplitudes I_n and grating coupling strengths g_n we can solve Eq. (3) for the parameters p_0, p_1, q_-, q_+ and with those calculate the transfer matrices S and Σ.

4. Fundamental Transformation Matrices

In this section we introduce a set of "fundamental" transformations that each couple two input and two output ports. As we will show in Section V, these fundamental operations can be concatenated, together with phase shifts, to achieve the most general 4×4 matrix operation that is possible in this system, in the same way as a universal *unidirectional* $N \times N$ optical transformation can be achieved as a sequence of directional waveguide couplers and phase shifters [10], [11].

The first two of these fundamental transformations can be implemented by standard Bragg gratings in single waveguides. For example, a Bragg grating in the bottom waveguide of Fig. 1 couples the inputs I_0 and I_2 leading to outputs O_0 and O_2, while the top waveguide modes are left unchanged ($O_3 = I_1$ and $O_1 = I_3$). Analogously, a grating in the top waveguide only couples the other inputs and outputs. The unidirectional matrices corresponding to these two operations can be derived from coupled mode theory and are given by

$$\Sigma_0(\phi) = \begin{bmatrix} \cosh(\phi) & \cdot & \sinh(\phi) & \cdot \\ \cdot & 1 & \cdot & \cdot \\ \sinh(\phi) & \cdot & \cosh(\phi) & \cdot \\ \cdot & \cdot & \cdot & 1 \end{bmatrix}, \quad \Sigma_1(\phi) = \begin{bmatrix} 1 & \cdot & \cdot & \cdot \\ \cdot & \cosh(\phi) & \cdot & \sinh(\phi) \\ \cdot & \cdot & 1 & \cdot \\ \cdot & \sinh(\phi) & \cdot & \cosh(\phi) \end{bmatrix} \tag{14}$$

for Bragg gratings in waveguide 0 and 1, respectively, and $\phi = g_B L/2$ where g_B is the coupling coefficient of the grating.

The next fundamental transformation is achieved by long-period waveguide grating couplers [16], [17] in both waveguides that couple the two waveguides modes to each other via a cladding mode. Eq. (7) leads to the corresponding unidirectional transformation matrix

$$\Sigma_2(\phi) = \begin{bmatrix} -\cos(\phi) & \sin(\phi) & \cdot & \cdot \\ \sin(\phi) & \cos(\phi) & \cdot & \cdot \\ \cdot & \cdot & -\cos(\phi) & \sin(\phi) \\ \cdot & \cdot & \sin(\phi) & \cos(\phi) \end{bmatrix} \tag{15}$$

where $\cos(\phi) = \frac{1-|\alpha|^2}{1+|\alpha|^2}$ and $\sin(\phi) = \frac{2|\alpha|}{1+|\alpha|^2}$ with $\alpha = -g_3/g_2$. Note that this operation couples the two forward propagating modes, but because of the reversibility of the device simultaneously couples the backward propagating modes in the same way.

The final fundamental 2×2 transformation in our system couples the forward propagating mode in one waveguide to the backward propagating mode in the other waveguide. This novel element consists of a long-period grating in one waveguide and a short-period grating in the other. The grating periods of the two gratings are carefully chosen such that both are precisely phase-matched at the same operating wavelength to a single cladding mode. For $|g_1| < |g_2|$ and with a device of length determined by Eqs. (4) and (6), we are able to couple light with practically any coupling ratio between the two waveguide modes under consideration. From Eq. (7) the corresponding

unidirectional transformation matrix is given by

$$\Sigma_3(\phi) = \begin{bmatrix} -\cosh(\phi) & \cdot & \cdot & \sinh(\phi) \\ \cdot & \cosh(\phi) & -\sinh(\phi) & \cdot \\ \cdot & \sinh(\phi) & -\cosh(\phi) & \cdot \\ -\sinh(\phi) & \cdot & \cdot & \cosh(\phi) \end{bmatrix} \tag{16}$$

where $\phi = 2\,\mathrm{arctanh}(g_1/g_2)$.

Note that for $\phi = 0$, both $\Sigma_2(0)$ and $\Sigma_3(0)$ represent a single long-period grating in waveguide 0 with the device length given by Eqs. (4) and (6). This leads to coupling of the light from waveguide 0 to the cladding mode and back, such that a π phase shift is achieved relative to the light in waveguide 1.

Finally, arbitrary phase shifts of light in a single waveguide can be achieved by off-resonant coupling to the cladding mode via a long-period grating or by directly modifying the propagation constant of the waveguide by fabricating it with a modified refractive index contrast. The unidirectional transformation matrices for phase shifts in waveguides 0 and 1 are

$$\Theta_0(\varphi) = \begin{bmatrix} \exp(i\varphi) & \cdot & \cdot & \cdot \\ \cdot & 1 & \cdot & \cdot \\ \cdot & \cdot & \exp(-i\varphi) & \cdot \\ \cdot & \cdot & \cdot & 1 \end{bmatrix}, \quad \Theta_1(\varphi) = \begin{bmatrix} 1 & \cdot & \cdot & \cdot \\ \cdot & \exp(i\varphi) & \cdot & \cdot \\ \cdot & \cdot & 1 & \cdot \\ \cdot & \cdot & \cdot & \exp(-i\varphi) \end{bmatrix}. \tag{17}$$

Note that again a phase shift will be induced in both the forward and the backward propagating mode at the same time.

We find the following properties of the matrices: $\Sigma_0(\phi)\cdot\Sigma_0(-\phi) = I$, $\Sigma_1(\phi)\cdot\Sigma_1(-\phi) = I$, $\Sigma_2(\phi)^2 = I$, $\Sigma_3(\phi)^2 = I$ where I is the 4×4 identity matrix in unidirectional space which corresponds to the light being entirely transmitted from each end of both waveguides to the other end. The first two relations predict that a standard Bragg grating with a π phase shift in the center transmits resonant light, as expected for a phase-shift grating Fabry-Perot resonator [30]–[32]. The final two relations follow from Eq. (7) and show that doubling the length of the device leads to an entire oscillation, $\cos(2\Omega L) = 1$, which leaves the light in its original state.

5. Construction of an Arbitrary Symmetric Unitary Matrix

By concatenating the fundamental operations discussed above, Eqs. (14)–(17), we can now build up more complex 4×4 couplers. Below we show that we can achieve any arbitrary matrix on this platform that is both *unitary and symmetric*, that is, any matrix S that satisfies the conditions

$$\begin{aligned} S^\dagger \cdot S &= I, \\ S &= S^T \end{aligned} \tag{18}$$

where T and $\dagger$ are the transpose and the conjugate transpose, respectively. The restriction to symmetric matrices is due to the time reversal property of light propagation. Using Eqs. (12) and (13) it can be shown that these conditions are equivalent to unidirectional matrices Σ of the form

$$\Sigma = \begin{bmatrix} P & Q^* \\ Q & P^* \end{bmatrix} \tag{19}$$

where P and Q are 2×2 matrices. Conservation of energy also implies

$$\begin{aligned} 1 &= |\sigma_{00}|^2 + |\sigma_{10}|^2 - |\sigma_{20}|^2 - |\sigma_{30}|^2, \\ 1 &= |\sigma_{01}|^2 + |\sigma_{11}|^2 - |\sigma_{21}|^2 - |\sigma_{31}|^2, \\ 0 &= \sigma_{00}^*\sigma_{01} + \sigma_{10}^*\sigma_{11} - \sigma_{20}^*\sigma_{21} - \sigma_{30}^*\sigma_{31}, \\ 0 &= \sigma_{00}\sigma_{21} + \sigma_{10}\sigma_{31} - \sigma_{20}\sigma_{01} - \sigma_{30}\sigma_{11}, \end{aligned} \tag{20}$$

where σ_{mn} are the elements of Σ.

We will first discuss the case of *real-valued* matrices of the form (18), i.e. the case of symmetric orthogonal matrices S. It can be seen that our four fundamental matrices (14)–(16) are of the form (19). Moreover, real matrices of the form (19) have 8 degrees of freedom (8 real matrix elements of P and Q) but 4 of them are constrained by Eqs. (20), thus leaving 4 independent degrees of freedom and therefore the same number as of our fundamental transformations.

Any arbitrary symmetric and orthogonal (i.e. real-valued) matrix S can be composed by a sequence of our fundamental 2×2 couplers (14)–(16) as follows.

- First, we apply Eq. (13) to convert S into its unidirectional form Σ.
- We apply the matrix $\Sigma_2(\phi)$, corresponding to a long-period grating waveguide coupler, to our matrix with ϕ chosen to set the matrix element σ_{10} to zero. Because of the matrix form (19) this also sets $\sigma_{32} = 0$.
- We apply the matrix $\Sigma_0(\phi)$, corresponding to a standard Bragg grating in waveguide 0, with ϕ chosen to set $\sigma_{20} = 0$. This also sets $\sigma_{02} = 0$ while leaving the matrix elements set to zero in the previous step unchanged.
- Next we apply the matrix $\Sigma_3(\phi)$, which corresponds to our new type of coupler with a long-period grating in one waveguide and a short-period grating in the other. Here we choose ϕ to set $\sigma_{30} = \sigma_{12} = 0$ without changing any of the matrix elements set to zero above. From Eqs. (20) and (19) follows also $\sigma_{01} = \sigma_{03} = \sigma_{23} = \sigma_{21} = 0$.
- Finally, we apply the matrix $\Sigma_1(\phi)$, corresponding to a standard Bragg grating in waveguide 1, with ϕ chosen such that $\sigma_{31} = \sigma_{13} = 0$. We are then left with a diagonal matrix, which can only have entries of ± 1 on the diagonal because of (20).

With this procedure we have therefore found a decomposition of any arbitrary symmetric and orthogonal transformation matrix S into a sequence of fundamental 2×2 couplers (apart from trivial phase shifts of ± 1 which could be corrected at the output ports O_n).

For complex-valued matrices S, a similar decomposition is possible if the matrix S is symmetric and *unitary*. In this case, before any of the matrices Σ_n ($n = 0, 1, 2, 3$) is applied in the decomposition procedure described above an additional phase shift needs to be applied by using one of the phase shift operations, Eq. (17), to make the relevant matrix elements real-valued.

6. Examples of Matrix Decompositions

Using the results of the previous section, we here present a few 4×4 transformations that are of interest for optical information processing and that can be realized in our platform.

As a first example, the Walsh-Hadamard gate S_W in the form

$$S_W = \frac{1}{2}\begin{bmatrix} 1 & 1 & 1 & 1 \\ 1 & -1 & 1 & -1 \\ 1 & 1 & -1 & -1 \\ 1 & -1 & -1 & 1 \end{bmatrix} \tag{21}$$

can be written in the unidirectional form Σ_W as a sequence of binary couplers as

$$\Sigma_W = \Sigma_2\left(-\frac{\pi}{4}\right) \cdot \Sigma_0\left(arctanh\left(\frac{1}{2}\right)\right) \cdot \Sigma_3\left(-\text{arctanh}\left(\frac{1}{\sqrt{3}}\right)\right) \cdot \Sigma_1\left(-\text{arctanh}\left(\frac{1}{2}\right)\right) \cdot \Theta_1(\pi), \tag{22}$$

Similarly, the 4×4 quantum Fourier transform S_{QFT}

$$S_{QFT} = \frac{1}{2}\begin{bmatrix} 1 & 1 & 1 & 1 \\ 1 & i & -1 & -i \\ 1 & -1 & 1 & -1 \\ 1 & -i & -1 & i \end{bmatrix} \tag{23}$$

is expressed in unidirectional form as

$$\Sigma_{QFT} = \Theta_0\left(\frac{\pi}{4}\right)\cdot\Theta_1\left(-\frac{\pi}{4}\right)\cdot\Sigma_2\left(\frac{\pi}{4}\right)\cdot\Theta_0\left(\frac{\arctan(\frac{1}{3})}{2}\right)\cdot\Sigma_0\left(-\text{arctanh}\left(\frac{\sqrt{10}}{4}\right)\right)$$
$$\cdot\Theta_0\left(\frac{-\arctan\left(\frac{1}{3}\right)}{2}\right)\cdot\Theta_1\left(-\frac{\pi}{4}\right)\cdot\Sigma_3\left(\text{arctanh}\left(\frac{1}{\sqrt{3}}\right)\right)\cdot\Theta_1\left(-\frac{\pi}{4}\right)$$
$$\cdot\Sigma_1\left(\text{arctanh}\left(\frac{1}{2}\right)\right)\cdot\Theta_1\left(\frac{\pi}{4}\right). \tag{24}$$

Various C-NOT transforms can also be implemented. Consider the form

$$S_{\text{CNOT},1} = \begin{bmatrix} 1 & 0 & 0 & 0 \\ 0 & 0 & 0 & 1 \\ 0 & 0 & 1 & 0 \\ 0 & 1 & 0 & 0 \end{bmatrix} \tag{25}$$

that gives $O_0 = I_0$, $O_2 = I_2$ and swaps $O_1 = I_3$ and $O_3 = I_1$. A simple Bragg grating in waveguide 0 in the limit of strong grating strength, $\Sigma_0(\phi \to \infty)$, gives

$$S_0(\phi \to \infty) = \begin{bmatrix} -1 & 0 & 0 & 0 \\ 0 & 0 & 0 & 1 \\ 0 & 0 & 1 & 0 \\ 0 & 1 & 0 & 0 \end{bmatrix} \tag{26}$$

which only requires a π phase shift at the output port O_0 to achieve $S_{\text{CNOT},1}$. A C-NOT gate of the form

$$S_{CNOT,2} = \begin{bmatrix} 1 & 0 & 0 & 0 \\ 0 & 1 & 0 & 0 \\ 0 & 0 & 0 & 1 \\ 0 & 0 & 1 & 0 \end{bmatrix} \tag{27}$$

can also be achieved (up to a π phase shift at the output O_0 again) as a sequence of two unidirectional operations

$$\Sigma_3(\phi \to \infty)\cdot\Sigma_0(\phi \to \infty), \tag{28}$$

i.e., a highly reflective Bragg grating in waveguide 0 followed by a strong coupler of the forward and backward modes between the two waveguides. Note that the matrix (27) cannot be converted by (13) because $S_{01} = 0$ but the conversion is possible in the limit of negligible but non-zero grating transmissions.

7. Numerical Results

In this section we discuss the implementation of the fundamental transformations introduced in Sec. IV in our physical platform, Fig. 1. The parameters used for the simulations are the same as in our previous work [20]. We use a refractive index of the cladding of 1.4398 (in practice, this would be the effective index of the slab mode of the core layer), a device width of 34.0 μm, two waveguides of Gaussian index profile with a $1/e$ half-width of 2.0 μm, a waveguide index contrast of 0.01 and placed at a distance of 10 μm from the center on both sides of the device. The operation wavelength is 1.55 μm. We compute the modes using 4001 grid points inside the ridge and also simulate an air layer of 5 μm outside of the ridge on either side to ensure correct boundary conditions.

This system has 46 different modes propagating in a single direction in total. Modes 0 and 1, as found using the finite differences method, are the symmetric and anti-symmetric core modes of

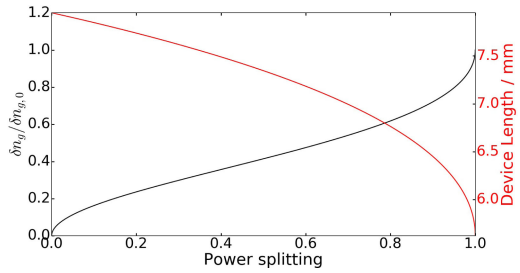

Fig. 2. Grating index contrast ratio (black) and device length required (red) for desired power at output O_3, normalised to input I_0, for a long-period waveguide grating coupler with $\Lambda_g = 6.202\ \mu$m, $\theta = 72.936^\circ$ and $\delta n_{g,0} = 0.001$.

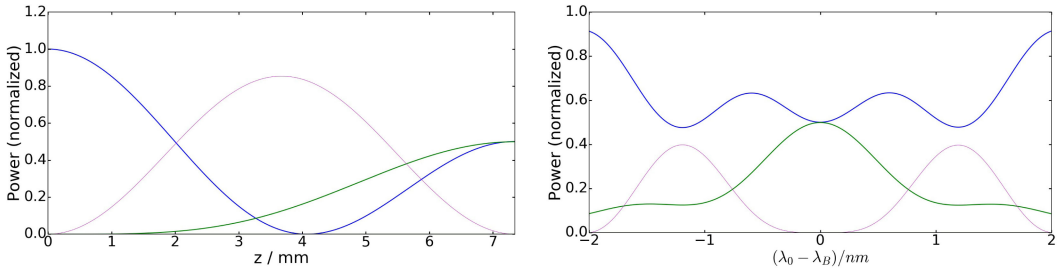

Fig. 3. (a) Power propagation along the forward propagating waveguide (blue and green) and cladding (magenta) modes for a 50:50 beam splitter from Fig. 2. (b) Power output per mode versus wavelength (same colors). Parameters as in Fig. 2 with $L = 7.346$ mm and grating index contrast $\delta n_g = 0.0004142$ in the second waveguide.

the device and have an effective index of 1.4445. As a "bus" cladding mode we use mode 35 with an effective refractive index of 1.1946. The grating periods are chosen to phase match the modes we want to couple longitudinally and the tilt angle is set to maximize the coupling coefficient. Thus, for standard Bragg gratings coupling counter-propagating waveguide modes the required grating period is 536.53 nm with a tilt angle of 0°. For short-period gratings coupling a waveguide mode with a counter-propagating cladding mode the period is 587.338 nm and the tilt angle 17.23°. Finally, for long-period gratings the period is 6.202 μm and the tilt angle is chosen as 72.936° which creates long-period gratings of equal coupling coefficient to short-period gratings with the same index contrast.

For standard Bragg gratings with a grating index contrast of $\delta n_g = 0.001$ we find a grating coupling coefficient $g_B = 2.637 \times 10^{-3}\ \mu\text{m}^{-1}$. Using Eq. (14) we find that a 50:50 power splitting is achieved by a 0.668 mm grating and a backreflection of 99% with a length of 2.270 mm. The full-width half-maximum bandwidth in the two cases are found to be 1.392 nm and 0.875 nm, respectively.

With our implementation of long-period waveguide-to-waveguide grating couplers we achieve a coupling coefficient of $g_2 = 7.903 \times 10^{-4}\ \mu\text{m}^{-1}$ between the core mode and the forward propagating cladding mode with a grating index contrast of $\delta n_g = 0.001$. However, to achieve a given power coupling ratio between the waveguide modes while also ensuring that no light is lost through the cladding mode at the device end facets we need to change both the device length and one of the grating strengths. Using the results of Sec. III, Fig. 2 shows the grating index contrasts and the device lengths needed to achieve any unidirectional power splitting. We see that device lengths are of the order of 6–8 mm for most couplers. As an example, a 50-50 beam splitter requires a grating index contrast $\delta n_g = 0.001$ in waveguide 0 and $\delta n_g = 0.0004142$ in waveguide 1 over a device length of $L = 7.346$ mm which is comparable to the lengths of the devices in [17], [18]. For this device, we also show in Fig. 3(a) the power in each mode along the device, clearly demonstrating that the power in the cladding mode vanishes at both ends. The dependence of the device output as the

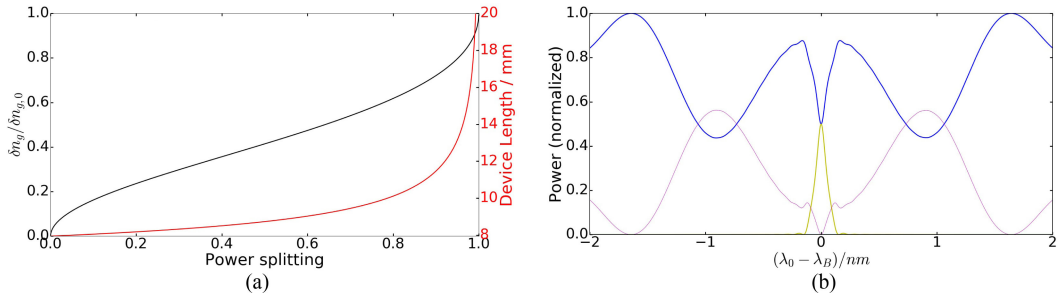

Fig. 4. (a) Grating index contrast ratio (black) and length (red) required for arbitrary power output O_2, normalised to input I_0, for the grating coupler with one long- and one short-period grating with $\Lambda_g = 6.202\ \mu$m, $\theta = 72.936^\circ$, and $\delta n_{g,0} = 0.001$ for the grating in waveguide 0 and $\Lambda_g = 587.338$ nm, $\theta = 17.23^\circ$, and δn_g in waveguide 1. (b) Wavelength dependence of output power in the forward propagating mode of waveguide 0 (blue), the backward propagating mode of waveguide 1 (yellow) and the forward propagating cladding mode (magenta) of the 50:50 beam splitter found in (a) with $\delta_{n,g} = 0.0004142$ and $L = 8.734$ mm.

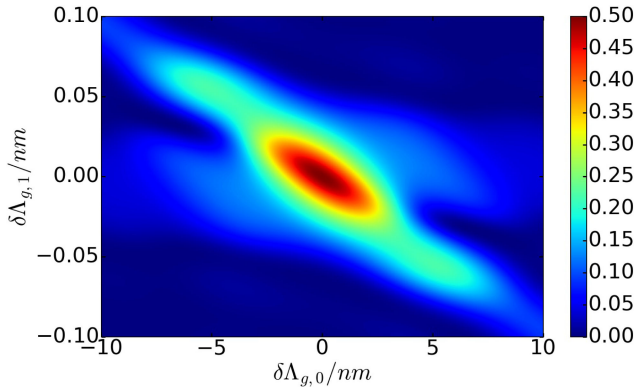

Fig. 5. Power output of the backward propagating mode of waveguide 1 of the 50:50 coupler from Fig. 4(b) as a function of variations of the long- and short-period grating periods $\delta\Lambda_{g,0}$ and $\delta\Lambda_{g,1}$, respectively. Light is launched into waveguide 0; parameters as in Fig. 4.

light wavelength is shifted away from the design wavelength is depicted in Fig. 3(b). We find that the full-width half-maximum bandwidth is 0.637 nm.

Next, we discuss the implementation of the device with a long-period grating in one waveguide and a short-period grating in the other to achieve any splitting ratio between light propagating forward in one waveguide and backward in the other waveguide. The required grating contrast ratios and device lengths calculated with the model of Sec. III are plotted in Fig. 4(a). Compared to the device with two long period gratings, Fig. 2, this new device typically requires longer device lengths of order 8–20 mm. The wavelength dependence of the corresponding 50:50 coupler is also shown in Fig. 4(b). In this case, we find a full-width half-maximum bandwidth of 0.0533 *nm*. We note that the bandwidth of this device is considerably smaller than that of the coupler with two long-period gratings shown previously in Fig. 3(b). This is due to the higher wavelength selectivity of the short period grating where a small change of light wavelength leads to a large change in the phase mismatch because of the counter-propagating nature of the coupled beams, whereas in a co-propagating long-period grating coupler the phase mismatch with changing wavelength is much smaller.

To show how precise our grating periods need to be in order to achieve this implementation of the long- and short-period waveguide coupler, we vary both grating periods around the optimized values for the 50:50 coupler of Fig. 4(b). The resulting power output of the backward propagating mode of waveguide 1 is shown in Fig. 5. We find that the device is much more sensitive to deviations

of the grating period of the short-period grating than to that of the long-period grating because of its greater wavelength selectivity, as already discussed above. To ensure correct device operation will therefore require very precise manufacturing of the gratings.

For comparison, with our current experimental setup [23]–[26] we estimate that the ridge structure can be micromachined to a precision of 1 μm and positioning of the waveguides with respect to the structure is accurate to about 100 nm. The central Bragg wavelength can be defined to a precision of around 0.05 nm. We thus expect that some active tuning, e.g. by temperature, may be required to achieve the accuracy required for the devices discussed in this paper.

8. Compact Walsh-Hadamard Transform

In Sec. V we found the most general class of transformations that our platform allows and showed how any such 4×4 coupler can be implemented as a sequence of more fundamental 2×2 couplers. However, such a concatenated device may be impractical to fabricate and sensitive to fabrication limits in each of the constituent fundamental couplers.

Here we demonstrate that it is possible to implement at least some transformations in a much more compact form. In particular, we discuss an alternative implementation of the Walsh-Hadamard transform of Sec. V using a single device of superimposed long- and short-period gratings in each waveguide. This solution requires that the two short-period gratings and one of the long-period gratings have the same coupling coefficient while the second long-period grating has a three times larger coupling coefficient. The two short-period gratings must be in phase with each other and the two long-period gratings must be out of phase. We therefore require

$$\begin{aligned} g_0 = g_1 = g_2 e^{i\psi}, \\ g_3 = -3g_2 \end{aligned} \tag{29}$$

where ψ is an arbitrary phase difference between the short- and long-period gratings. We note that we also found another implementation of the Walsh-Hadamard gate where all gratings have coupling coefficients of equal amplitude and both sets of gratings are in phase. However, as seen in Eq. (4), such a solution is at the interface between the oscillatory and exponential regimes, which leads to an extremely narrow device bandwidth and sensitivity to fabrication imperfections.

In the following we consider the solution of Eq. (29) with $\psi = 0$. Using Eqs. (7)–(9), we find that the transformation matrix relating the outputs to the inputs is

$$S_M = \frac{1}{2}\begin{bmatrix} 1 & -1 & 1 & 1 \\ -1 & -1 & 1 & -1 \\ 1 & 1 & 1 & -1 \\ 1 & -1 & -1 & -1. \end{bmatrix}. \tag{30}$$

By applying a couple of trivial transformations in the form of a π phase shift at the output O_3 and the input I_1, and by swapping the inputs I_0 and I_2 (i.e., re-labeling them) we recover a Walsh-Hadamard gate of the form

$$\Upsilon_{O,3} \cdot S_M \cdot \Upsilon_{I,1} \cdot \Lambda_{I,02} = \frac{1}{2}\begin{bmatrix} 1 & 1 & 1 & 1 \\ 1 & 1 & -1 & -1 \\ 1 & -1 & 1 & -1 \\ 1 & -1 & -1 & 1 \end{bmatrix} \tag{31}$$

where

$$\Upsilon_{O,3} = \begin{bmatrix} 1 & . & . & . \\ . & 1 & . & . \\ . & . & 1 & . \\ . & . & . & -1 \end{bmatrix}, \quad \Upsilon_{I,1} = \begin{bmatrix} 1 & . & . & . \\ . & -1 & . & . \\ . & . & 1 & . \\ . & . & . & 1 \end{bmatrix}, \quad \Lambda_{I,02} = \begin{bmatrix} . & . & 1 & . \\ . & 1 & . & . \\ 1 & . & . & . \\ . & . & . & 1 \end{bmatrix}. \tag{32}$$

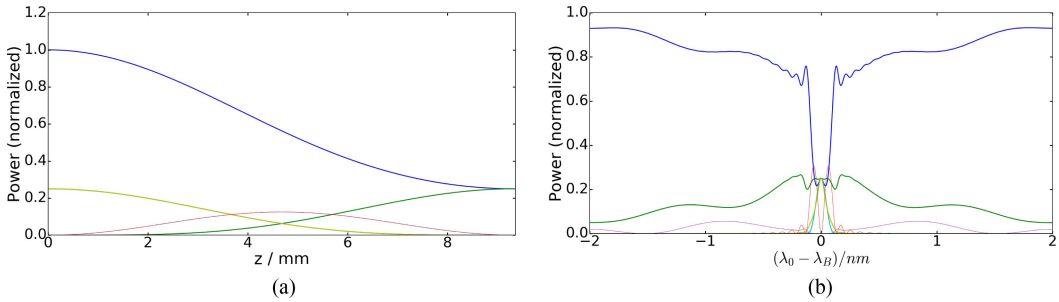

Fig. 6. Compact Walsh-Hadamard gate. (a) Power propagation along the forward propagating waveguide modes (blue and green), backward waveguide modes (cyan and yellow) and along the forward and backward propagating cladding mode (magenta and red). (b) Power outputs of the same modes versus wavelength. Here $\delta_{n,g} = 0.0003$ and $\theta = 17.23^\circ$ for the short-period gratings in both waveguides, $\theta = 72.936^\circ$ for the long-period gratings with $\delta_{n,g} = 0.0003$ in waveguide 0 and $\delta_{n,g} = 0.0009$ with a grating phase-shift of π, in waveguide 1. Light is launched in waveguide 0, device length is $L = 9.364$mm.

Fig. 6(a) shows the power flow between the device modes when power is launched into one of the waveguide modes. As expected, all four output ports then contain 25% of the launched input power while no power exits through the cladding mode at the end facets of the device. The corresponding wavelength dependence is shown in Fig. 6(b). Similar to the device containing one short- and one long-period grating, Fig. 4, this Walsh-Hadamard transform has a limited operating bandwidth of 0.0480 nm, full-width half-maximum and calculated using the power backreflected at output O_1, because of the wavelength selectivity of the short-period grating. This implementation of the Walsh-Hadamard transform is more compact than the one in [19] because it requires only two as opposed to four waveguides.

Solutions like the one of Eq. (29) for the Walsh-Hadamard gate can be found for arbitrary transformation matrices either by systematic parameter sweeps of coupling coefficients, similar to the figures of Sec. VII, or by numerical optimization, e.g., using Newton's method or the basin-hopping method. However, in contrast to the systematic approach described in Sec. V there is in general no guarantee that such optimization algorithms will converge. In general, the solutions that we find using this method can all be built using the "fundamental" transformations we introduce in Sec. IV.

9. Conclusion

We have proposed and analyzed the use of counter-propagating modes in an integrated silica waveguide structure for linear optical processing of fiber-coupled narrowband light for applications in quantum networks. Allowing light to propagate in both directions effectively doubles the number of available modes compared to unidirectional propagation devices. For the specific case of two coupled single-mode waveguides, i.e., two forward and two backward propagating modes, we have shown the class of 4×4 couplers that can be implemented is given by matrices that are both unitary and symmetric. A simple recipe has been presented to decompose any such transformation matrix into a linear sequence of 2×2 couplers and single-waveguide phase shifters.

We have also presented a physical implementation of the scheme by an integrated photonic device with UV-written waveguides and both short- and long-period grating couplers and discussed the parameters and device performance of the different types of 2×2 couplers. Instead of concatenating fundamental couplers, more complex transformations can also be achieved by direct superpositions of short- and long-period gratings, as we demonstrated with a compact Walsh-Hadamard transform.

The data used in this article is openly available at [33].

References

[1] F. Flamini, N. Spagnolo, and F. Sciarrino, "Photonic quantum information processing: A review," *Rep. Prog. Phys.*, vol. 82, 2019, Art. no. 016001.
[2] M. G. Thompson, A. Politi, J. C. F. Matthews, and J. L. O'Brien, "Integrated waveguide circuits for optical quantum computing," *IET Circ. Devices Syst.*, vol. 5, no. 2, pp. 94–102, 2011.
[3] F. Flamini *et al.*, "Thermally reconfigurable quantum photonic circuitsat telecom wavelength by femtosecond lasermicromachining," *Light. Sci. Appl.*, vol. 4, 2015, Art. no. e354.
[4] J. Carolan *et al.*, "Universal Linear Optics," *Science*, vol. 349, no. 6249, pp. 711–716, 2015.
[5] A. Politi, J. C. F. Matthews, M. G. Thompson, and J. L. O'Brien, "Integrated Quantum Photonics," *IEEE J. Sel. Topics Quantum Electron.*, vol. 15, no. 6, pp. 1673–1684, Nov./Dec. 2009.
[6] A. Crespi *et al.*, "Integrated photonic quantum gates for polarization qubits," *Nat. Commun.*, vol. 2, 2011, Art. no. 556.
[7] X. Qiang *et al.*, "Large-scale silicon quantum photonics implementing arbitrary two-qubit processing," *Nat. Photon.*, vol. 12, pp. 543–539, 2018.
[8] A. Crespi *et al.*, "Suppression law of quantum states in a 3D photonic fast Fourier transform chip," *Nat. Commun.*, vol. 7, 2016, Art. no. 10469.
[9] N. C. Harris *et al.*, "Quantum transport simulations in a programmable nanophotonic processor," *Nat. Photon.*, vol. 11, pp. 447–452, 2017.
[10] M. Reck, A. Zeilinger, H. J. Bernstein, and P. Bertani, "Experimental realization of any discrete unitary operator," *Phys. Rev. Lett.*, vol. 73, no. 1, pp. 58–63, 1994.
[11] C.-K. Li, R. Roberts, and X. Yin, "Decomposition of unitary matrices and quantum gates," *Int. J. Quantum. Inf.*, vol. 11, 2013, Art. no. 1350015.
[12] W. R. Clements, P. C. Humphreys, B. J. Metcalf, W. S. Kolthammer, and I. A. Walmsley, "Optimal design for universal multiport interferometers," *Optica*, vol. 3, no. 12, pp. 1460–1465, 2016.
[13] D. Marcuse, "Directional couplers made of nonidentical asymmetric slabs. Part II: Grating-assisted couplers," *J. Lightw. Technol.*, vol. 5, no. 2, pp. 268–273, 1987.
[14] D. Mechin, P. Grosso, and D. Bosc, "Add drop multiplexer with UV-written Bragg gratings and directional coupler in SiO_2 Si integrated waveguides," *J. Lightw. Technol.*, vol. 19, no. 9, pp. 1282–1286, 2001.
[15] W. Shi *et al.*, "Ultra-compact, flat-top demultiplexer using anti-reflection contra-directional couplers for CWDM networks on silicon," *Opt. Exp.*, vol. 21, no. 6, pp. 6733–6738, Mar 2013.
[16] Y. Bai and K. S. Chiang, "Analysis and design of long-period waveguide-grating couplers," *J. Lightw. Technol.*, vol. 23, no. 12, pp. 4363–4373, 2005.
[17] Y. Bai, Q. Liu, K. P. Lor, and K. S. Chiang, "Widely tunable long-period waveguide grating couplers," *Opt. Exp.*, vol. 14, no. 26, pp. 2595–2597, 2006.
[18] K. C. Chow, K. S. Chiang, Q. Liu, K. P. Lor, and H. P. Chan, "UV-written long-period waveguide grating coupler for broadband add/drop multiplexing," *Opt. Commun.*, vol. 282, no. 184, pp. 378–381, 2009.
[19] S.-Y. Tseng, "Synthesis of a 4×4 Walsh-Hadamard transformer using long-period waveguide grating arrays," *IEEE Photon. Techol. Lett.*, vol. 21, no. 14, pp. 972–974, 2009.
[20] M. J. Weisen, M. T. Posner, J. C. Gates, B. E. Gawith, P. G. R. Smith, and P. Horak, "Low-loss wavelength-selective integrated waveguide coupler based on tilted Bragg gratings," *J. Opt. Soc. Amer. B*, vol. 36, no. 7, pp. 1783–1791, 2019.
[21] H. J. Kimble, "The quantum internet," *Nature*, vol. 453, pp. 1023–1030, 2008.
[22] D. Zauner, K. Kulstad, J. Rathje, and M. Svalgaard, "Directly uv-written silica-on-silicon planar waveguides with low insertion loss," *Electron. Lett.*, vol. 34, no. 16, pp. 1582–1584, 1998.
[23] H. L. Rogers, S. Ambran, C. Holmes, P. G. R. Smith, and J. C. Gates, "*In situ* loss measurement of direct UV-writtenwaveguides using integrated Bragg gratings," *Opt. Lett.*, vol. 35, no. 17, pp. 2849–2851, 2010.
[24] P. C. Gow, R. H. S. Bannerman, P. L. Mennea, C. Holmes, J. C. Gates, and P. G. R. Smith, "Direct UV written integrated planar waveguides using a 213 nm laser," *Opt. Exp.*, vol. 27, no. 20, pp. 29 133–29 137, Sep. 2019. [Online]. Available: https://www.osapublishing.org/abstract.cfm?URI=oe-27-20-29133
[25] C. Sima *et al.*, "Ultra-wide detuning planar Bragg grating fabrication technique based on direct UV grating writing with electro-optic phase modulation," *Opt. Exp.*, vol. 21, no. 13, pp. 15 747–15 754, 2013.
[26] C. Holmes, L. G. Carpenter, H. L. Rogers, I. J. G. Sparrow, J. C. Gates, and P. G. R. Smith, "Planar waveguide tilted Bragg grating refractometer fabricated through physical micromachining and direct UV writing," *Opt. Exp.*, vol. 19, no. 13, pp. 12 462–8, 2011.
[27] K. Okamoto, *Fundamentals of Optical waveguides*, 2nd ed. Amsterdam, The Netherlands: Elsevier, 2005.
[28] M. T. Posner *et al.*, "Integrated polarizer based on 45° tilted gratings," *Opt. Exp.*, vol. 27, no. 8, pp. 11 174–11 181, 2019.
[29] G. K. Svendsen, M. W. Haakestad, and J. Skaar, "Reciprocity and the scattering matrix of waveguide mode," *Phys. Rev. A*, vol. 87, 2013, Art. no. 013838.
[30] L. Poladin, B. Ashton, W. E. Padden, A. Michie, and C. Marra, "Characterisation of phase-shifts in gratings fabricated by over-dithering and simple displacement," *Opt. Fiber Technol.*, vol. 9, no. 4, pp. 173–188, 2003.
[31] J. Zhou *et al.*, "Novel fabrication technique for phase-shifted fiber Bragg gratings using a variable-velocity scanning beam and a shielded phase mask," *Opt. Exp.*, vol. 26, no. 10, 2018, Art. no. 13311.
[32] Y. Zhao *et al.*, "Study on the characters of phase-shifted fiber Bragg grating in asymmetric perturbation and its application in fiber laser acoustic sensor," *Photonic Sens.*, vol. 8, no. 4, pp. 351–357, 2018.
[33] M. J. Weisen, J. C. Gates, C. B. E. Gawith, P. G. R. Smith, and P. Horak, "4-by-4 integrated waveguide coupler based on bi-directional propagation in two single-mode waveguides (dataset)," University of Southampton, 2019, https://doi.org/10.5258/SOTON/D1639.